

# Road Extraction by Deep Residual U-Net

Zhengxin Zhang<sup>1</sup>, Qingjie Liu<sup>1</sup>, *Member, IEEE*, and Yunhong Wang, *Senior Member, IEEE*

**Abstract**—Road extraction from aerial images has been a hot research topic in the field of remote sensing image analysis. In this letter, a semantic segmentation neural network, which combines the strengths of residual learning and U-Net, is proposed for road area extraction. The network is built with residual units and has similar architecture to that of U-Net. The benefits of this model are twofold: first, residual units ease training of deep networks. Second, the rich skip connections within the network could facilitate information propagation, allowing us to design networks with fewer parameters, however, better performance. We test our network on a public road data set and compare it with U-Net and other two state-of-the-art deep-learning-based road extraction methods. The proposed approach outperforms all the comparing methods, which demonstrates its superiority over recently developed state of the arts.

**Index Terms**—Convolutional neural network, deep residual U-Net, road extraction.

## I. INTRODUCTION

**R**OAD extraction is one of the fundamental tasks in the field of remote sensing. It has a wide range of applications such as automatic road navigation, unmanned vehicles, urban planning, and geographic information update. Although it has been received considerable attentions in the past decade, road extraction from high-resolution remote sensing images is still a challenging task, because of the noise, occlusions, and complexity of the background in raw remote sensing imagery.

A variety of methods have been proposed to extract roads from remote sensing images in recent years. Most of these methods can be divided into two categories: road area extraction and road centerline extraction. Road area extraction [1]–[6] can generate pixel-level labeling of roads, while road centerline extraction [7], [8] aims at detecting skeletons of a road. There are also methods that extract both road areas and centerline, simultaneously [9]. Since road centerline can be easily obtained from road areas using algorithms such as morphological thinning [10], this letter focuses on road area extraction from high-resolution remote sensing images.

Road area extraction can be considered as a segmentation or pixel-level classification problem. For instance, Song and Civco [11] proposed a method utilizing shape index feature and support vector machine (SVM) to detect road areas. Das *et al.* [12] exploited two salient features of roads and designed a multistage framework to extract roads

from high-resolution multispectral images using probabilistic SVM. Alshehhi and Marpu [6] proposed an unsupervised road extraction method based on hierarchical graph-based image segmentation.

Recent years have witnessed great progress in deep learning. Methods based on deep neural networks have achieved state-of-the-art performance on a variety of computer vision tasks, such as scene recognition [13] and object detection [14]. Researchers in remote sensing community also seek to leverage the power of deep neural networks to solve the problems of interpretation and understanding of remote sensing data [2], [5], [15]–[18]. These methods provide better results than traditional ones, showing great potential of applying deep learning techniques to analyze remote sensing tasks.

In the field of road extraction, one of the first attempts of applying deep learning techniques was made by Mnih and Hinton [2]. They proposed a method employing restricted Boltzmann machines (RBMs) to detect road areas from high-resolution aerial images. To achieve better results, a preprocessing step before the detection and a postprocessing step after the detection were applied. The preprocessing was deployed to reduce the dimensionality of the input data. The postprocessing was employed to remove disconnected blotches and fill in the holes in the roads. Different from Mnih and Hinton's method [2] that uses RBMs as basic blocks to build deep neural networks, Saito *et al.* [5] employed convolutional neural networks to extract buildings and roads directly from raw remote sensing imagery. This method achieves better results than Mnih and Hinton's method [2] on the Massachusetts roads data set.

Recently, lots of works have suggested that a deeper network would have better performance [19], [20]. However, it is very difficult to train a very deep architecture due to problems such as vanishing gradients. To overcome this problem, He *et al.* [21] proposed the deep residual learning framework that utilizes an identity mapping [22] to facilitate training. Instead of using skip connection in fully convolutional networks [23], Ronneberger *et al.* [24] proposed the U-Net that concatenates feature maps from different levels to improve segmentation accuracy. U-Net combines low-level detail information and high-level semantic information, thus achieving promising performance on biomedical image segmentation [24].

Inspired by the deep residual learning [21] and U-Net [24], in this letter, we propose the deep residual U-Net, an architecture that takes advantage of strengths from both deep residual learning and U-Net architecture. The proposed deep residual U-Net (ResUnet) is built based on the architecture of U-Net. The differences between our deep ResUnet and U-Net are in twofold. First, we use residual units instead of plain neural units as basic blocks to build the deep ResUnet. Second, the cropping operation is unnecessary, thus removed from our

Manuscript received June 1, 2017; revised August 23, 2017, November 4, 2017, and December 17, 2017; accepted January 9, 2018. Date of publication March 8, 2018; date of current version April 20, 2018. This work was supported by the Natural Science Foundation of China under Grant 61601011. (Zhengxin Zhang and Qingjie Liu contributed equally to this work.) (Corresponding author: Qingjie Liu.)

The authors are with the State Key Laboratory of Virtual Reality Technology and Systems, School of Computer Science and Engineering, Beihang University, Beijing 100191, China (e-mail: qingjie.liu@buaa.edu.cn).

Color versions of one or more of the figures in this letter are available online at <http://ieeexplore.ieee.org>.

Digital Object Identifier 10.1109/LGRS.2018.2802944



TABLE I  
NETWORK STRUCTURE OF RESUNET

	Unit level	Conv layer	Filter	Stride	Output size
Input					$224 \times 224 \times 3$
Encoding	Level 1	Conv 1	$3 \times 3/64$	1	$224 \times 224 \times 64$
		Conv 2	$3 \times 3/64$	1	$224 \times 224 \times 64$
	Level 2	Conv 3	$3 \times 3/128$	2	$112 \times 112 \times 128$
		Conv 4	$3 \times 3/128$	1	$112 \times 112 \times 128$
	Level 3	Conv 5	$3 \times 3/256$	2	$56 \times 56 \times 256$
		Conv 6	$3 \times 3/256$	1	$56 \times 56 \times 256$
Bridge	Level 4	Conv 7	$3 \times 3/512$	2	$28 \times 28 \times 512$
		Conv 8	$3 \times 3/512$	1	$28 \times 28 \times 512$
	Level 5	Conv 9	$3 \times 3/256$	1	$56 \times 56 \times 256$
		Conv 10	$3 \times 3/256$	1	$56 \times 56 \times 256$
	Level 6	Conv 11	$3 \times 3/128$	1	$112 \times 112 \times 128$
		Conv 12	$3 \times 3/128$	1	$112 \times 112 \times 128$
Decoding	Level 7	Conv 13	$3 \times 3/64$	1	$224 \times 224 \times 64$
		Conv 14	$3 \times 3/64$	1	$224 \times 224 \times 64$
Output		Conv 15	$1 \times 1$	1	$224 \times 224 \times 1$

decoding.<sup>1</sup> The first part encodes the input image into compact representations. The last part recovers the representations to a pixel-wise categorization, i.e., semantic segmentation. The middle part serves like a bridge connecting the encoding and decoding paths. All of the three parts are built with residual units that consist of two  $3 \times 3$  convolution blocks and an identity mapping. Each convolution block includes a BN layer, a ReLU activation layer, and a convolutional layer. The identity mapping connects input and output of the unit.

Encoding path has three residual units. In each unit, instead of using pooling operation to downsample the feature map size, a stride of 2 is applied to the first convolution block to reduce the feature map by half. Correspondingly, decoding path also comprises three residual units. Before each unit, there is an upsampling of feature maps from lower level and a concatenation with the feature maps from the corresponding encoding path. After the last level of decoding path, a  $1 \times 1$  convolution and a sigmoid activation layer is used to project the multichannel feature maps into the desired segmentation. In total, we have 15 convolutional layers comparing with 23 layers of U-Net. It is worth noting that the indispensable cropping in U-Net is unnecessary in our network. The parameters and output size of each step are presented in Table I.

### B. Loss Function

Given a set of training images and the corresponding ground truth segmentations  $\{I_i, s_i\}$ , our goal is to estimate parameters  $W$  of the network, such that it produce accurate and robust road areas. This is achieved through minimizing the loss between the segmentations generated by  $\text{Net}(I_i; W)$  and the ground truth  $s_i$ . In this letter, we use mean squared error as the loss function

$$\mathcal{L}(W) = \frac{1}{N} \sum_{i=1}^N \|\text{Net}(I_i; W) - s_i\|^2, \quad (3)$$

where  $N$  is the number of the training samples. We use the stochastic gradient descent (SGD) to train our network. One should know that other loss functions that are derivable can also be used to train the network. For instance, U-Net adopted pixel-wise cross entropy as loss function to optimize the model.

<sup>1</sup>U-Net used “contracting” and “expansive” paths to denote the feature extraction and up-convolution stages of the network. In this letter, we prefer the terms encoding and decoding because we think it is more meaningful and easier to understand.

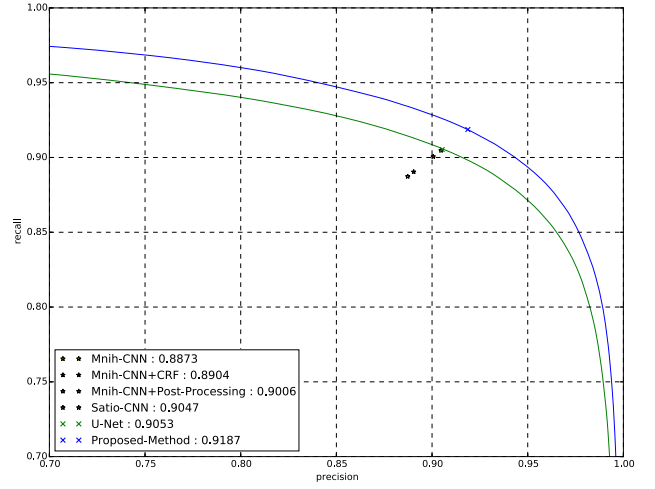


Fig. 3. Relaxed precision-recall curves of U-Net and the proposed method on Massachusetts roads data set. The marks ‘\*’ and ‘x’ are break-even points of different methods.

### C. Result Refinement

The input and output of our semantic segmentation network have the same size in width and height, both are  $224 \times 224$ . The pixels near boundaries of the output have lower accuracy than center ones due to zero padding in the convolutional layer. To get a better result, we use an overlap strategy to produce the segmentation results of a large image. The input subimages are cropped from the original image with an overlap of  $o$ . The final results are obtained by stitching all subsegmentations together. The values in the overlap regions are averaged.

## III. EXPERIMENTS

To demonstrate the accuracy and efficiency of the proposed deep ResUnet, we test it on Massachusetts roads data set<sup>2</sup> and compare it with three state of the art methods, including Mnih’s [2] method, Saito’s method [5], and U-Net [24].

### A. Data Set

The Massachusetts roads data set was built by Mihn and Hinton [2]. The data set consists of 1171 images in total, including 1108 images for training, 14 images for validation, and 49 images for testing. The size of all the images in this data set is  $1500 \times 1500$  pixels with a resolution of 1.2 m/pixel. This data set roughly covers 500-km<sup>2</sup> space crossing from urban, suburban to rural areas, and a wide range of ground objects including roads, rivers, sea, various buildings, vegetations, schools, bridges, ports, and vehicles. In this letter, we train our network on the training set of this data set and report results on its test set.

### B. Implementation Details

The proposed model was implemented using Keras [25] and optimized by minimizing (3) through the SGD algorithm. There are 1108 training images sized  $1500 \times 1500$  available for training. Theoretically, our network can take arbitrary size image as input; however, it will need amount of GPU memory to store the feature maps. In this letter, we utilize fixed-sized training images ( $224 \times 224$  as described in Table I) to train the

<sup>2</sup><https://www.cs.toronto.edu/~vmnih/data/>



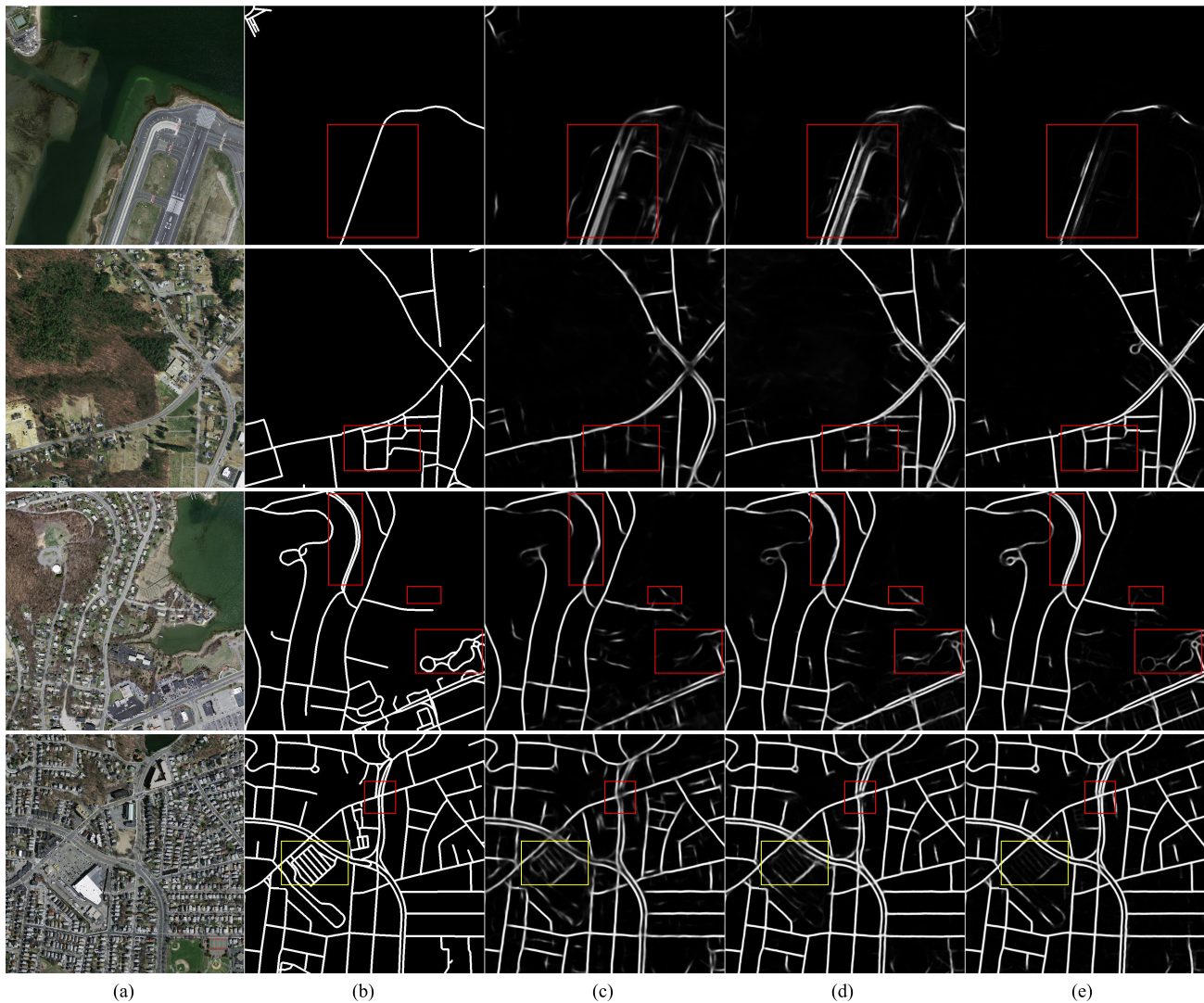


Fig. 4. Example results on the test set of Massachusetts roads data set. (a) Input image. (b) Ground truth. (c) Saito *et al.* [5]. (d) U-Net [24]. (e) Proposed ResUnet. Zoomed-in view to see more details.

model. These training images are randomly sampled from the original images. At last, 30 000 samples are generated and fed into the network to learn the parameters. It should be noted that no data augmentation is used during training. We start training the model with a minibatch size of 8 on an NVIDIA Titan 1080 GPU with 8 GB onboard memory.<sup>3</sup> The learning rate was initially set to 0.001 and reduced by a factor of 0.1 in every 20 epochs. The network will converge in 50 epochs. We set overlap  $o = 14$  in our experiments, as it exhibits a good speed accuracy tradeoff.

### C. Evaluation Metrics

The most common metrics for evaluating a binary classification method are precision and recall. In remote sensing, these metrics are also called correctness and completeness. The precision is the fraction of predicted road pixels, which are labeled as roads, and the recall is the fraction of all the labeled road pixels that are correctly predicted.

<sup>3</sup>Other relevant hardware including E5 2630 CPU, 96-GB RAM, and 4-TB HDD. The OS is Ubuntu 14.04.

Because of the difficulty in correctly labeling all the road pixels, Mnih and Hinton [2] introduced the relaxed precision and recall scores [26] into road extraction. The relaxed precision is defined as the fraction of number of pixels predicted as road within a range of  $\rho$  pixels from pixels labeled as road. The relaxed recall is the fraction of number of pixels labeled as road that are within a range of  $\rho$  pixels from pixels predicted as road. In this experiment, the slack parameter  $\rho$  is set to 3, which is consistent with previous studies [2], [5]. We also report break-even points of different methods. The break-even point is defined as the point on the relaxed precision-recall curve, where its precision value equals its recall value. In other words, break-even point is the intersection of precision-recall curve and line  $y = x$ .

### D. Comparisons

Comparisons with three state-of-the-art deep-learning-based road extraction methods are conducted on the test set of Massachusetts roads data set. The break-even points of the proposed and comparing methods are reported in Table II. Fig. 3 presents the relaxed precision-recall curves of U-Net

TABLE II

COMPARISONS OF THE PROPOSED AND OTHER THREE DEEP-LEARNING-BASED ROAD EXTRACTION METHODS ON MASSACHUSETTS ROAD DATA SET IN TERMS OF BREAK-EVEN POINT. A HIGHER BREAK-EVEN POINT INDICATES A BETTER PERFORMANCE IN PRECISION AND RECALL

Model	Break-even point
Mnih-CNN [2]	0.8873
Mnih-CNN+CRF [2]	0.8904
Mnih-CNN+Post-Processing [2]	0.9006
Saito-CNN [5]	0.9047
U-Net [24]	0.9053
ResUnet	<b>0.9187</b>

and our network and their break-even points, along with break-even points of comparing methods. It can be seen that our method performs better than all other three approaches in terms of relaxed precision and recall. Although the parameters of our network are only 1/4 of U-Net (7.8 versus 30.6 M), promising improvement are achieved on the road extraction task.

Fig. 4 illustrates four example results of Saito *et al.* [5], U-Net [24], and the proposed ResUnet. It can be seen that our method shows cleaner results with less noise than the other two methods. Especially when there are two-lane roads, our method can segment each lane with high confidence, generating clean, and sharp two-lane roads, while other methods may confuse lanes with each other, as demonstrated in the third row of Fig. 4. Similarly, in the intersection regions, our method also produces better results.

Context information is very important when analyzing objects with complex structures. Our network considers context information of roads, thus can distinguish roads from similar objects such as building roofs, and airfield runways. From the first row of Fig. 4, we can see that, even the runway has very similar features to a highway, our method can successfully segment side road from the runway. In addition to this, the context information also makes it robust to occlusions. For example, parts of the roads on the rectangle of the second row are covered by trees. Saito's method and U-Net cannot detect road under the trees; however, our method labeled them successfully. A failure case is shown in the yellow rectangle of the last row. Our method missed the roads in the parking lot. This is mainly because most of roads in parking lots are not labeled. Therefore, although these roads share the same features to the normal ones, considering the context information our network regard them as backgrounds.

#### IV. CONCLUSION

In this letter, we have proposed the ResUnet for road extraction from high-resolution remote sensing images. The proposed network combines the strengths of residual learning and U-Net. The skip connections within the residual units and between the encoding and decoding paths of the network will facilitate information propagations both in forward and backward computations. This property not only eases training, but also allows designing simple yet powerful neural networks. The proposed network outperforms U-Net with only 1/4 of its parameters, as well as other two state-of-the-art deep-learning-based road extraction methods.

#### REFERENCES

- [1] X. Huang and L. Zhang, "Road centreline extraction from high-resolution imagery based on multiscale structural features and support vector machines," *Int. J. Remote Sens.*, vol. 30, no. 8, pp. 1977–1987, 2009.
- [2] V. Mnih and G. E. Hinton, "Learning to detect roads in high-resolution aerial images," in *Proc. ECCV*, 2010, pp. 210–223.
- [3] C. Unsalan and B. Sirmacek, "Road network detection using probabilistic and graph theoretical methods," *IEEE Trans. Geosci. Remote Sens.*, vol. 50, no. 11, pp. 4441–4453, Nov. 2012.
- [4] G. Cheng, Y. Wang, Y. Gong, F. Zhu, and C. Pan, "Urban road extraction via graph cuts based probability propagation," in *Proc. ICIP*, Oct. 2015, pp. 5072–5076.
- [5] S. Saito, T. Yamashita, and Y. Aoki, "Multiple object extraction from aerial imagery with convolutional neural networks," *Electron. Imag.*, vol. 60, no. 10, pp. 1–9, 2016.
- [6] R. Alshehhi and P. R. Marpu, "Hierarchical graph-based segmentation for extracting road networks from high-resolution satellite images," *ISPRS J. Photogramm. Remote Sens.*, vol. 126, pp. 245–260, Apr. 2017.
- [7] B. Liu, H. Wu, Y. Wang, and W. Liu, "Main road extraction from ZY-3 grayscale imagery based on directional mathematical morphology and VGI prior knowledge in urban areas," *PLoS ONE*, vol. 10, no. 9, p. e0138071, 2015.
- [8] C. Sujatha and D. Selvathi, "Connected component-based technique for automatic extraction of road centerline in high resolution satellite images," *EURASIP J. Image Video Process.*, vol. 2015, no. 1, p. 8, 2015.
- [9] G. Cheng, Y. Wang, S. Xu, H. Wang, S. Xiang, and C. Pan, "Automatic road detection and centerline extraction via cascaded end-to-end convolutional neural network," *IEEE Trans. Geosci. Remote Sens.*, vol. 55, no. 6, pp. 3322–3337, Jun. 2017.
- [10] G. Cheng, F. Zhu, S. Xiang, and C. Pan, "Road centerline extraction via semisupervised segmentation and multidirectional nonmaximum suppression," *IEEE Geosci. Remote Sens. Lett.*, vol. 13, no. 4, pp. 545–549, Apr. 2016.
- [11] M. Song and D. Civco, "Road extraction using SVM and image segmentation," *Photogramm. Eng. Remote Sens.*, vol. 70, no. 12, pp. 1365–1371, 2004.
- [12] S. Das, T. T. Mirmalinee, and K. Varghese, "Use of salient features for the design of a multistage framework to extract roads from high-resolution multispectral satellite images," *IEEE Trans. Geosci. Remote Sens.*, vol. 49, no. 10, pp. 3906–3931, Oct. 2011.
- [13] B. Zhou, A. Lapedriza, J. Xiao, A. Torralba, and A. Oliva, "Learning deep features for scene recognition using places database," in *Proc. NIPS*, 2014, pp. 487–495.
- [14] S. Ren, K. He, R. Girshick, and J. Sun, "Faster R-CNN: Towards real-time object detection with region proposal networks," *IEEE Trans. Pattern Anal. Mach. Intell.*, vol. 39, no. 6, pp. 1137–1149, Jun. 2017.
- [15] V. Mnih and G. E. Hinton, "Learning to label aerial images from noisy data," in *Proc. ICML*, 2012, pp. 567–574.
- [16] Q. Zhang, Y. Wang, Q. Liu, X. Liu, and W. Wang, "CNN based suburban building detection using monocular high resolution Google Earth images," in *Proc. IGARSS*, Jul. 2016, pp. 661–664.
- [17] L. Zhang, L. Zhang, and B. Du, "Deep learning for remote sensing data: A technical tutorial on the state of the art," *IEEE Geosci. Remote Sens. Mag.*, vol. 4, no. 2, pp. 22–40, Jun. 2016.
- [18] Z. Zhang, Y. Wang, Q. Liu, L. Li, and P. Wang, "A CNN based functional zone classification method for aerial images," in *Proc. IGARSS*, Jul. 2016, pp. 5449–5452.
- [19] C. Szegedy *et al.*, "Going deeper with convolutions," in *Proc. CVPR*, Jun. 2015, pp. 1–9.
- [20] K. Simonyan and A. Zisserman, "Very deep convolutional networks for large-scale image recognition," Unpublished paper, 2014. [Online]. Available: <https://arxiv.org/abs/1409.1556>
- [21] K. He, X. Zhang, S. Ren, and J. Sun, "Deep residual learning for image recognition," in *Proc. CVPR*, Jun. 2016, pp. 770–778.
- [22] K. He, X. Zhang, S. Ren, and J. Sun, "Identity mappings in deep residual networks," in *Proc. ECCV*, 2016, pp. 630–645.
- [23] J. Long, E. Shelhamer, and T. Darrell, "Fully convolutional networks for semantic segmentation," in *Proc. CVPR*, Apr. 2015, pp. 3431–3440.
- [24] O. Ronneberger, P. Fischer, and T. Brox, "U-Net: Convolutional networks for biomedical image segmentation," in *Proc. MICCAI*, 2015, pp. 234–241.
- [25] F. Chollet *et al.* (2015). *Keras*. [Online]. Available: <https://github.com/fchollet/keras>
- [26] M. Ehrig and J. Euzenat, "Relaxed precision and recall for ontology matching," in *Proc. Workshop Integr. Ontol.*, 2005, pp. 25–32.